doi.org/10.36721/PJPS.2024.37.5.REG.1135-1150.1

An untargeted UPLC-Q-TOF-MS-based plasma metabonomics revealed the effects of peperomin E in a prostate cancer nude mouse model

Shanshan Ma, Shuaishuai Wang and Yunzhi Li*
School of Pharmacy, Anhui University of Chinese Medicine, Hefei, China

Abstract: *Peperomia dindygulensis* is used as an anticancer medicinal plant in China and is rich in a series of novel secolignans, including peperomin E (PE). In our prior study, we demonstrated the significant reduction in tumor weight and volume *in vivo* in a PCa DU145 cell xenograft tumor mouse model following PE treatment. However, the impact of PE on PCa metabolism remains unclear. Therefore, the objective of this investigation is to examine the influence of PE on metabolism regulation within a PCa mouse model. An untargeted UPLC-Q-TOF-MS plasma metabolomics approach was carried out to explore the mechanism of action of PE in a human prostate cancer DU145 cell xenograft tumour mouse model based on principal component analysis (PCA), partial least squares discriminant analysis (PLS-DA), identification of potential biomarkers and pathway analysis. A total of 71 potential plasma metabolite biomarkers were identified in the nude mouse model and 36 of which were reversed to different degrees after the treatment with PE. These identified biomarkers primarily relate to amino acid metabolism, fatty acid metabolism and cholic acid metabolism. These findings showed that PE could improve endogenous metabolism in the DU145 cell xenograft tumor mouse model and offered a reliable foundation for the design of new therapeutic drugs for treating PCa.

Keywords: Lignans, bioactivity, metabonomics, UPLC-Q-TOF-MS, untargeted.

Submitted on 17-04-2023 – Revised on 27-05-2024 – Accepted on 15-07-2024

INTRODUCTION

Prostate cancer (PCa) ranks among the top 2 cancers in men and the 5th in morbidity around the world (Bray, *et al*., 2018). Though China is not a high-incidence district, with changes in dietary habits, the morbidity of PCa in China is increasing. The data showed that the incidence of PCa was the 7th most common male malignancy in China and the 10th most common morbidity (Chen, *et al*., 2016). Although many drugs have raised the survival rate of patients with PCa in recent years, there are still many deficiencies (Han, *et al*., 2015). Therefore, it is urgent to research and develop new anti-PCa drugs.

Peperomin E (PE) is one of secolignans first obtained from *Peperomia dindygulensis*. Miq. (Piperaceae) which used as an anti-tumor herbs in China (Lin, *et al*., 2021; Lin, *et al*., 2011). Our previous investigations also isolated PE from *Peperomia cavaleriei* C.DC (Li, *et al*., 2018). Previous studies have suggested that PE had a significant inhibitory effect on a variety of tumor cell lines *in vitro*, such as PC-3, HL-60, A549, VA-13, HepG2, HONE-1, LoVo, MCF-7 and NUGC-3 (Lin, *et al*., 2021; Li, *et al*., 2019). To screen the potential active compound against PCa, we studied its activity on cell and animal model and found that PE could suppress the proliferation of both PC-3 and DU145 prostate cancer cells *in vitro* and reduce tumor volume and decrease tumor weight *in vivo* in a DU-145 mouse xenograft tumor model, which displayed its potential anti-PCa activity (Lin, *et al*., 2021; Li, *et al*., 2019).

Recently, more and more evidences showed that metabolic disorders were closely related to tumorigenesis, and targeting tumor metabolism and regulating the cancer metabolic machine has arisen as a promising strategy for cancer therapy. The previous investigation also showed that metabolic disorder existed in the patients with PCa (Luzzago, *et al*., 2021). Therefore, it is of great significance to screen and find compounds that can regulate the disordered metabolism in patients with prostate cancer. Currently, metabonomics has become a powerful tool to discover possible biomarkers by analysing metabolites of low molecular weight from cells, tissues or organisms, and which has been successfully applied in multiple fields of pharmaceutical research, such as effectiveness evaluation, mechanism of action and therapeutic material basis. Currently, two technical platforms are commonly used in metabonomics research: NMR and LC-MS or GC-MS. Because of its advantages in sensitivity, LC-MS is widely used in metabonomics.

So far, it is unknown whether PE affects metabolite regulation in PCa. Hence, we carried out a LC-MS based untargeted metabonomics to assess the metabolic regulation of PE in a PCa nude mouse model (fig. 1).

MATERIALS AND METHODS

**Corresponding authors:* e-mails: yunzhili@live.com

Chemicals and reagents

PE was isolated from *P. cavaleriei* (Li, *et al*., 2018). Acetonitrile (chromatographic grade) was procured from Merck (Darmstadt, Germany), while methanol (chromatographic grade) was sourced from Sigma-Aldrich (St. Louis, MO, USA). Formic acid was obtained from Fluka (Buchs, Switzerland) and all other chemicals were of analytical grade. Distilled water from Watsons was utilized for all experiments.

Animals and cells

Male BALB/c nude mice (5 weeks old, weighing 18-20 g) were procured from Sippr-BK (Shanghai, China) for use in the study. The human DU145 prostate cancer cell was purchased from BeNa Culture Collection (Beijing, China). Foetal bovine plasma (FBS) was obtained from Gibco-BRL (Gaithersburg, MD, USA). RPMI-1640 medium was provided by HyClone (Logan, UT, USA).

Mouse xenograft study

Our research adhered to the guidelines outlined by the National Institutes of Health concerning the care and utilization of laboratory animals. Each mouse was individually housed in metabolic cages within a specific pathogen-free animal facility, maintained at a constant room temperature ranging between 23-25°C and relative humidity of 40-60%. A standard 12/12 hour light-dark cycle was maintained, and mice were provided with ad libitum access to standard mouse chow and water throughout the study. A week later, the mice were randomly divided into two parts: part one (n = 12) and part two (n = 24). The animals of part one were used as the normal control and the mice of part two were used to establish the orthotopic tumor transplantation model. After 15 days of feeding, the mice of part two was furthermore divided randomly into two groups: Group one was used as the tumor control which only administered normal 0.9% sodium chloride saline solution, while group two served as group of drug treatment which was intraperitoneally (IP) treated with 25 mg/kg PE (Lin, *et al*., 2021). Following daily administration for 24 consecutive days, the mice were euthanized via exsanguination and blood was promptly collected from the abdominal cavity into heparinized tubes. Following centrifugation at 13,000 rpm at 4°C for 15 minutes, the plasma obtained from the blood samples was stored at -80°C until subjected to LC-MS analysis.

The sample preparation and UPLC-MS analysis

The thawed plasma samples (50µL) were combined with 150µL of methanol containing 2-chloro-L-phenylalanine (12.5µg/mL) as an internal standard and vortexed for 1 minute. After centrifugation at 13,000 rpm at 4°C for 15 minutes, 100µL of the supernatant was transferred into an injection vial and 3µL was used for LC-MS analysis.

UPLC analysis was performed using an Agilent 1290 II Infinity LC system coupled with a 6545 UHD Accurate-Mass Q-TOF mass spectrometer (Agilent, USA). Separation utilized an ACQUITY UPLC HSS T3 column (2.1 × 100 mm, 2.5µm, Waters, MA, USA) using a mobile phase composed of 0.1% aqueous methanoic acid (A) and acetonitrile containing 0.1% methanoic acid (B), at a rate of 0.35mL/min. The chromatographic gradient was optimized as follows: starting from 0% phase B, ramping to 5% from 0 to 2 minutes, further ramping from 5% to 95% phase B from 2 to 13 minutes and maintaining 95% phase B from 13 to 15 minutes. A post-time of 5 minutes was set for system re-equilibration.

This study employed electrospray ionization (ESI) for MS analysis in both positive and negative polarities, employing the following optimized parameters: capillary voltage set at 4 kV and 3.5 kV for positive and negative mode, respectively, fragment voltage at 120 V, skimmer voltage at 60 V, nebulizer pressure at 45 psig, drying gas flow rate at 11 L/min and gas temperature maintained at 350°C (Fei *et al*., 2016). The acquisition range spanned from 100 to 1100 m/z. Additionally, to ensure the accuracy of the mass axis, reference ions were simultaneously injected into the mass spectrometer, with ions set at 922.0098 and 121.0509 for positive ion mode, and 1033.9881 and 112.9856 for negative ion mode. Quality control (QC) samples were employed to assess system stability.

Potential biomarkers identification and metabolic pathway analysis

The extracted molecular weights of metabolites were compared to online metabolite databases (Human Metabolome Database, METLIN) to find their possible identities. The structures of the putative metabolites were identified by comparing with MS/MS information from these databases. The metabolite identification confidence level is moderate (level 2 confidence). The metabolic pathways related to potential biomarkers were analysed using Metabo Analyst 3.0.

ETHICAL APPROVAL

The procedures for animal experiments adhered to relevant national laws and local guidelines, receiving approval from the Animal Ethics Committee of Guizhou Medical University on March 2, 2019 (Approval No: 1900220).

STATISTICAL ANALYSIS

The MS raw data underwent conversion to the mzXML format utilizing Mass Hunter Qualitative Analysis Software (Agilent Technologies). Subsequently, data pre-processing was conducted using the XCMS program within the R software platform, encompassing peak identification, retention time correction and peak integration.

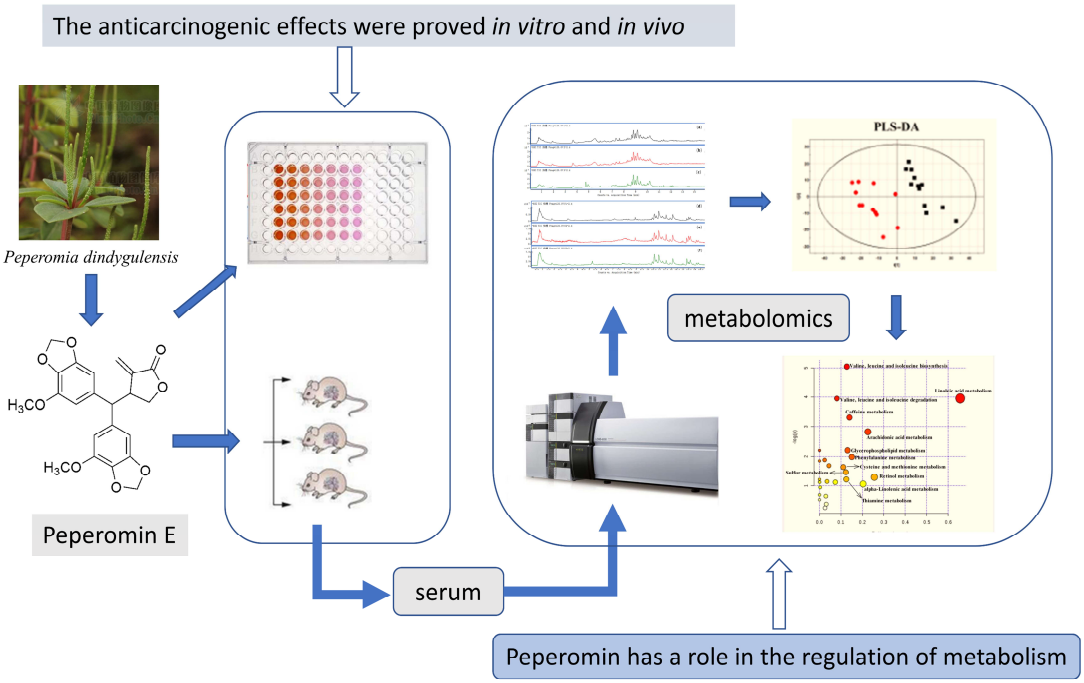

Fig. 1: The experimental scheme of UPLC-Q-TOF-MS-based plasma metabonomics for investigating the effects of peperomin E in a prostate cancer nude mouse model.

Following filtering the ion based on the 80% rule, where ions present in 80% of the samples within each group were deemed endogenous metabolites, relative metabolite quantities were determined by normalizing to the peak area of the internal standard (Fei *et al*., 2016). Mean-centering and Pareto scaling were then applied, and the retention time (RT)–m/z pair, relative ion intensity, and observation name were imported into SIMCA-P 11.0 software (Umetrics, Umea, Sweden) for multivariate data analysis (Fei *et al*., 2016). Model fitting was visually assessed using a permutation test. Potential biomarkers were identified based on variable importance in projection (VIP) values greater than 1.0 and p-values less than 0.05. The analysis employed VIP values from the PLS-DA model (threshold >1), in conjunction with three sets of ANOVA analyses followed by pairwise Tukey tests (panova <0.05, p1-2 <0.05), to discern differentially expressed metabolites between the normal and model groups. Additionally, Receiver Operating Characteristic (ROC) curves were constructed to evaluate the sensitivity and specificity of potential markers (Fei *et al*., 2016).

Experimental data were statistically analyzed using SPSS software (version 19.0, Chicago, IL, USA), with results reported as mean ± standard deviation (SD). A p value < 0.05 was considered to be significant.

RESULTS

Metabolic profiling analysis of plasma

To elucidate the underlying mechanism of PE's protective effects, we conducted UPLC-Q-TOF-MS-based plasma metabonomics in a nude mouse xenograft model established with DU145 cells. Initially, we generated typical plasma total ion current (TIC) chromatograms from normal, model and treatment groups in both positive and negative ization modes.

Exemplary LC-MS chromatograms from each group are depicted in fig. S1. While differences among these groups were directly observable from the chromatograms, pattern recognition approaches such as PCA and PLS-DA were utilized to visually discern changes between groups. Typically, QC samples were employed to assess instrument status and system stability through the clustering degree of QC samples. In our study, a PCA score plot of test samples and QC samples demonstrated high aggregation in all QC samples, indicating system stability (fig. S2).

Subsequently, PLS-DA score plots were utilized to compare the normal with model groups and the model group with the treatment group. We separately analyzed the normal group (1) and model group (2) samples using the PLS-DA model, with score plots shown in fig. 2 for both positive and negative ion modes. Key parameters for assessing the discriminant model quality included R2 (representing model explanatory power) and Q2 values (representing model predictive power). For the positive ion mode, cumulative R2X = 0.22, R2Y = 0.903 and Q2 = 0.383; for the negative ion mode, cumulative R2X = 0.432, R2Y = 0.885 and Q2 = 0.679.

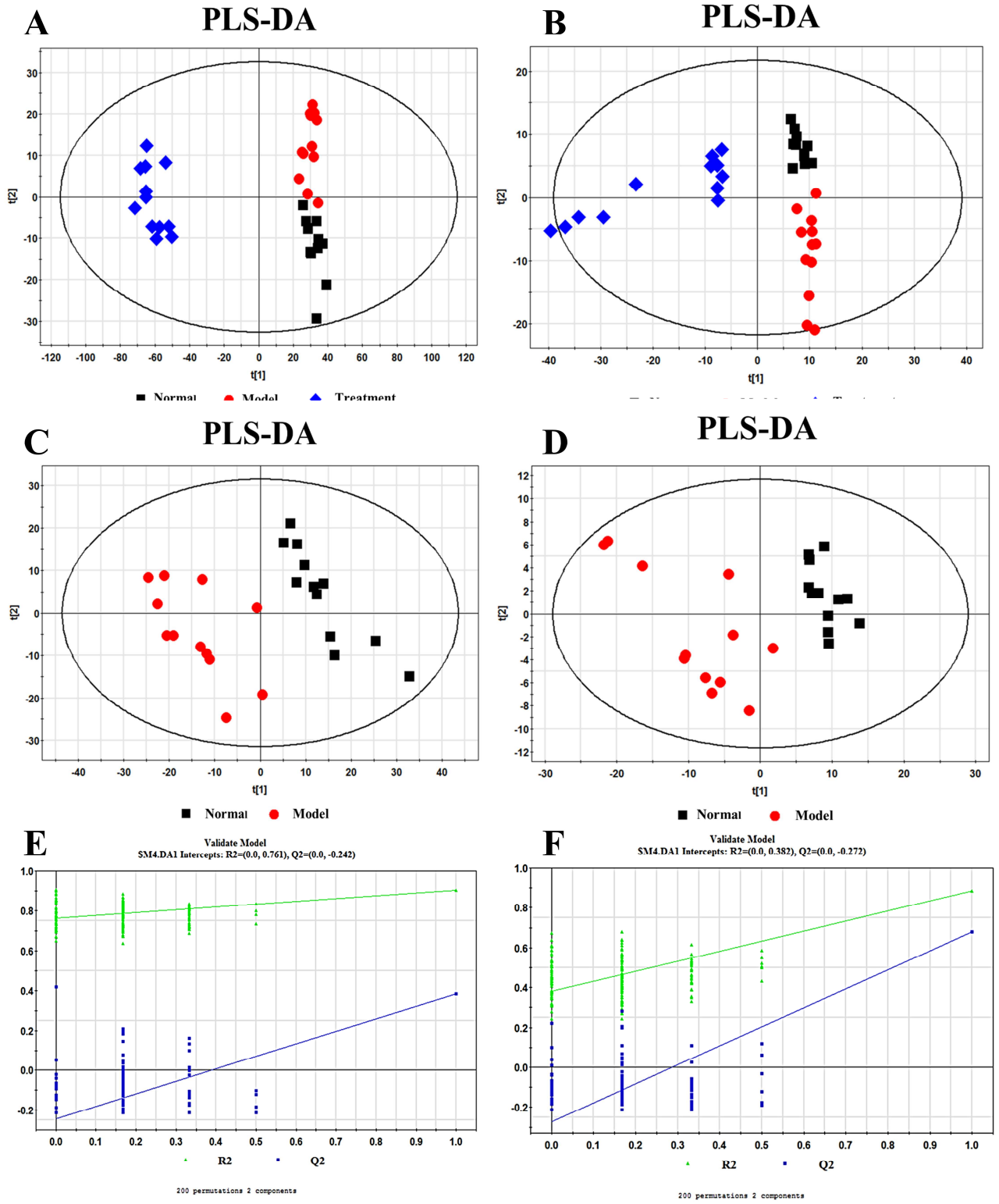

Fig. 2: The partial least squares discriminant analysis (PLS-DA) modeling was used to differentiate the metabolomic patterns of three groups (normal group, model group and treatment group) in ESI positive (A) and negative-ion modes (B) (■, Normal; ●, Model; ◆, Treatment). PLS-DA was used to differentiate the metabolomic patterns of two groups (normal group and model group) in ESI positive (C) and negative-ion modes (D) (■, Normal; ●, Model). Validation of the PLS-DA model in ESI positive (E) and negative-ion modes (F).

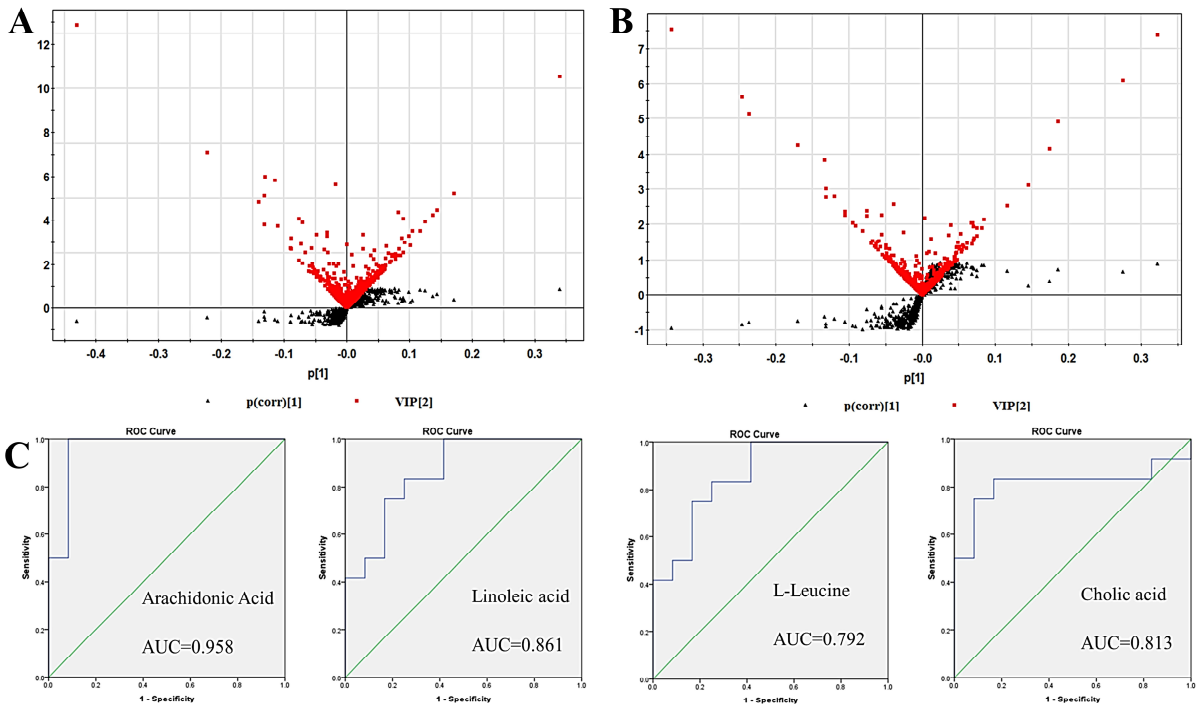

Fig. 3: Scatter and variable importance in projection (VIP) plots coupled with the VIP value plot of the model and the normal group in ESI positive (A) and negative-ion modes (B) (▲, p; ■, VIP). Representative results of Receiver Operating Characteristic (ROC) analysis and AUC for potential biomarkers of PCa (C).

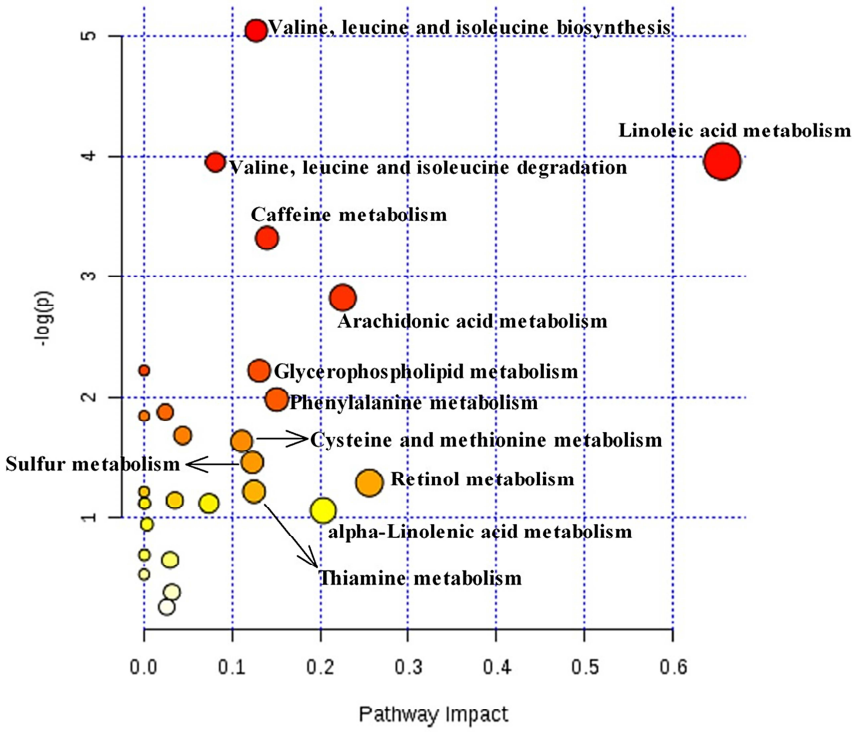

Fig. 4: Metabo Analyst 3.0 was used to analysed the significant metabolic pathways based on the biomarkers identified in the plasma of the model group (The vertical axis represents the p-value of the metabolic pathway test. The horizontal axis represents the rich factor, which is calculated by dividing the number of metabolites in the pathway enrichment set by the number in the background set. The size of the bubbles represents the number of differential metabolites involved in the pathway, while the color of the bubbles indicates the p-value of the metabolic pathway. The larger these two factors, the redder the color. The larger the bubble, the greater the number of metabolites enriched in that pathway).

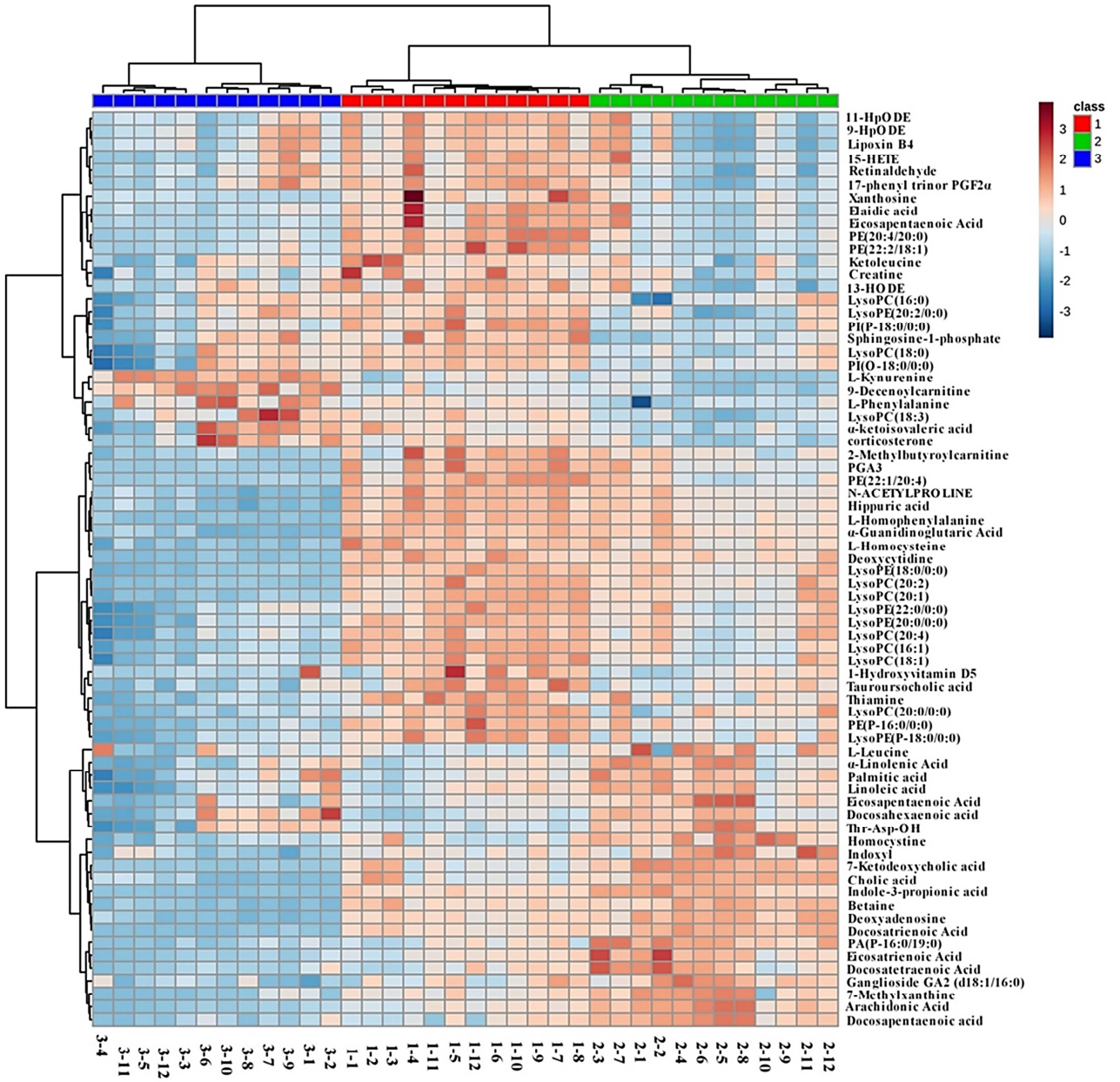

Fig. 5: Heat map of significantly altered metabolites in the normal, model and treatment groups.(1, ■, Normal; 2, ■, Model; 3, ■, Treatment.)

As depicted in fig. 2A, 2B, 2C and 2D, clear separation was observed between the model group and the normal group, as well as between the model group and the treatment group in both positive and negative ion modes, indicating significant differences. Furthermore, permutation tests were conducted to assess model over fitting, revealing no overfitting in either ESI positive or negative-ion mode (fig. 2E, 2F).

Biomarkers identification and metabolic pathway analysis

It is important to identify the potential significant metabolites which altered the metabolic profile of the DU145 nude mouse xenograft model. In this experiment, a scatter plot and a VIP were used to determine the difference in metabolites between the model and normal groups (fig. 3A, 3B). In addition, ANOVA and Tukey's post hoc test were further used to evaluate the data in the model group with those in the other two groups. In this paper, the metabolites with $p<0.05$ together with VIP values above 1 were considered potential biomarkers. According to the VIP value and the data of statistical analysis, a total of 71 potential metabolites (30 from positive-ion mode and 41 from negative-ion mode) were recognized (table S1, Supporting Information). Among them, the levels of 6 out of 30 differential metabolites in

positive-ion mode were increased in the model group compared to those in the normal group, while the levels of the remaining 24 metabolites were decreased. Similarly, the levels of 16 of 41 differential metabolites in negative-ion mode were increased, and the other metabolites were decreased compared to those in the normal group, respectively. In addition, these 71 biomarkers were further evaluated their potential for predictive and diagnostic performance in PCa by ROC analysis, and the data suggested that all of the candidate biomarkers had good diagnostic and predictive value based on the area under the ROC curve (AUC) >0.75 (fig. 3C).

Finally, Metabo Analyst 3.0 was used to carry out the biochemical interpretation of all altered metabolites. To identify the most relevant metabolic pathways, the p-value was set to 0.05 and the threshold for impact value in pathway topology analysis was established at 0.10, respectively. As shown in fig. 4, linoleic acid metabolism, valine, leucine and isoleucine biosynthesis, valine, leucine and isoleucine degradation, caffeine metabolism, arachidonic acid metabolism, glycerophospholipid metabolism, phenylalanine metabolism, cysteine and methionine metabolism, sulfur metabolism, α-linolenic acid metabolism, retinol metabolism and thiamine metabolism pathways were disrupted in the model.

The effects on metabolism regulation of PE

There were 71 metabolic biomarkers that were altered in the plasma of model mice and whether these metabolic biomarkers were regulated by PE intervention remains unclear. According to the fold change and p values between the treatment group and model group (table S1), 36 of the 71 metabolites in the treatment group had different levels of call back compared with the model group: α-ketoisovaleric acid, betaine, L-leucine, indoxyl, 7-methylxanthine, indole-3-propionic acid, L-kynurenine, deoxyadenosine, palmitic acid, homocysteine, α-linolenic acid, linoleic acid, retinaldehyde, 13-HODE, eicosapentaenoic acid, arachidonic acid, eicosatrienoic acid, 9-HpODE, 11-HpODE, 9-decenoylcarnitine, docosahexaenoic acid, docosapentaenoic acid, docosatetraenoic acid, docosatrienoic acid, corticosterone, lipoxin B4, Thr-Asp-OH, sphingosine-1-phosphate, 17-phenyl trinor PGF2α, 7-ketodeoxycholic acid, cholic acid, LysoPE (20:2/0:0), LysoPC (18:3), PA (P-16:0/19:0), ganglioside GA2 (d18:1/16:0) and L-phenylalanine. The variation trends of these 71 metabolites were also visualized using a heat map (fig. 5). The relevant metabolic pathways of these metabolites were analyzed using the KEGG pathway database and the results revealed that linoleic acid metabolism, valine, leucine and isoleucine biosynthesis, valine, leucine and isoleucine degradation, caffeine metabolism, arachidonic acid metabolism, phenylalanine metabolism and cysteine and methionine metabolism were regulated in the treatment group (fig. S3-S9), indicating that these pathways might be closely related to the protective effects of PE.

DISCUSSION

Secolignans are novel lignans that have been found in nature in recent years. Previous reports showed that PE exhibited good inhibitory activity against some cancer cell lines *in vitro* and *in vivo* (Lin, *et al*., 2021; Wang, *et al*., 2016). To screen the potential anti-PCa active compound, we also investigated its bioactivity, and found that PE could effectively inhibit the cellular proliferation of human PCa DU145 cells *in vitro* and decreased the tumor weight as well as the tumor volume *in vivo* (Lin, *et al*., 2021).

Recently, an increasing number of investigations have shown that the Gleason score of PCa patients with metabolic abnormalities (such as obesity, hypertension, and diabetes) was significantly increased and a higher degree of malignancy, demonstrating that metabolite alterations are closely related to the development of PCa (Luzzago, *et al*., 2021). In the study of endogenous small molecular components *in vivo*, metabonomics has unique advantages which can identify metabolic pathways significantly altered in disease, then obtain the pathogenesis of the disease and mechanism of a drug from a holistic view. Generally, there are three kinds of cell lines used in PCa research, among which the DU145 cell line is hormone-independent prostatic cancer cell line and is considered to be the standard prostate cancer cell line used widely in therapeutic research (Lin, *et al*., 2021; Sachan, *et al*., 2018; Zhang, *et al*., 2019). To date, there was no metabonomics report on the DU145 cell xenograft model. Hence, the effect of PE on metabolism regulation in a DU145 prostate cancer cell xenograft model was investigated by metabonomics in this experiment. Firstly, PLS-DA score plots showed that there was an obvious separation between the model group and the normal group (fig. 2a, 2b), indicating the significant difference in metabolites between them. Nevertheless, there is no overlap between the treatment group compared with the normal group, indicating that there are certain differences in metabolites between these two groups. In fact, the later differential metabolites analysis showed that there were 71 components in the model group changed significantly, of which 36 were corrected in the treatment group. So, drug intervention only led to the callback of some metabolites, there was still a difference between the treatment group and the normal group. In addition, the five blue spots (treatment group) are separated from the rest of the group, which showed that the metabolites of these animals are different from other animals in this group under the negative ion model.

Firstly, we investigated the metabolic disturbance and identified 71 metabolites as potential biomarkers for the nude mouse DU145 cell xenograft model, which is the first reported the change of metabolites in the DU145 cell xenograft model. Then, our investigation further found

that 36 of 71 metabolites were regulated after PE intervention and the metabolic pathways of these regulated metabolites are mainly related to the metabolism of fatty acids, amino acids, bile acid.

Previous investigations have shown that fatty acid anabolism plays a role in many tumorigenesis and developmental biological processes, including the formation of the cell membrane skeleton, energy storage, generation of signal molecules, and participation in many important functions of cells, etc., and metabolic reprogramming combined with the Warburg effect can adapt to the rapid growth of tumors (Senga, *et al*., 2018). Dyslipidaemia is also a marker of prostate cancer (Poulose, *et al*., 2018). More and more studies have shown that fatty acid metabolism is involved in the occurrence and progression of PCa (Watt *et al*., 2019). In surgical specimens of PCa, the expression of fatty acid synthases (FAS) was significantly higher than that of surrounding normal tissues and the expression of Fas increased gradually during the malignant process of prostate epithelial tissue, which participates in the formation of biomembranes to meet the high levels of cell proliferation and metabolism. This suggests that FAS play a key role in the proliferation and invasion of prostate cancer (Cortesi, *et al*., 2018). In this experiment, arachidonic acid was identified as a biomarker. Arachidonic acid is a polyunsaturated omega-6 fatty acid with important physiological significance. Previous investigations have suggested that a derivative of arachidonic acid could promote tumor angiogenesis by stimulating growth factors. Its main mechanism of action is that prostaglandin E2 (PGE2) can be produced from arachidonic acid by cyclooxygenase and PGE2 is the most important prostaglandin for angiogenesis (Hoang, *et al*., 2015). Lipoxin B4 and 15-HETE are also derivatives of arachidonic acid under the action of lipoxygenase and omega hydroxylase, respectively (Salvado, *et al*., 2012). Both of these derivatives decreased in the model mouse, suggesting that maladjustment of arachidonic acid metabolism occurred in the prostate cancer xenograft model. In addition, a previous investigation demonstrated that arachidonic acid get involved in the induction of androgen biosynthesis in prostate cancer cells under androgen deprivation, which partly explains the generation of castration resistance in prostate cancer (Yang, *et al*., 2012). Moreover, metabolic pathway analysis suggested that linoleic acid metabolism was the most important metabolic pathway related to the pathogenesis of prostate cancer, and linoleic acid is a precursor of arachidonic acid (Taha, *et al*., 2017). These two metabolites were significantly up regulated in the model whereas significantly down regulated in the treated mice in this experiment (table S1), indicating that inhibition of linoleic acid metabolism is an important mechanism of PE against prostate cancer.

Amino acid metabolism is another important way to affect the progression of prostate cancer (Chen, *et al*., 2023). The previous investigation found that nitrogen in tumor tissue increased significantly in metastatic prostate cancer tissue compared with normal prostate tissue due to the decomposition of amino acids. Our experiment also highlighted that amino acid metabolism plays a crucial role in the pathogenesis of prostate cancer, aligning with findings from previous research (Lucarelli *et al*., 2015). Specifically, the study revealed a significant connection between the biosynthesis and degradation of valine, leucine, and isoleucine and the development of prostate cancer. These branched chain amino acids (BCAAs) are not only essential for the synthesis of nitrogenous cellular components but also serve as signaling molecules. They are involved in the regulation of glucose and lipid metabolism, protein synthesis and immune responses through specific signaling networks, notably the PI3K/AKT/mTOR pathway (Nie *et al*., 2018). Previous investigations have also shown that the PI3K/AKT/mTOR signalling pathway play an important role in the occurrence and development of PCa (Claudio, *et al*., 2016). Therefore, our results suggested that valine, leucine and isoleucine metabolism play an important role in regulating energy homeostasis, immunity and disease in humans and animals. Furthermore, these amino acids were regulated in the treatment group, indicating that PE acts on experimental models by modulating amino acid metabolism.

In addition to the above two metabolic pathways, careful analysis of significantly changed metabolites in the plasma of the mouse model and treatment groups (table S1) revealed that the level of cholic acid (CA) increased significantly in the model and decreased significantly in the treatment group. CA is a primary bile acid (BA). After being synthesized in the liver, CA is transferred to the bile for secretion and then released to the intestine under the stimulation of gastrointestinal hormones. (Gallimore and Godkin, 2013), which can then absorb via intestinal cells to complete enterohepatic circulation by the portal vein system. Hence, CA is a substrate of the intestinal flora. The biotransformation of BA mainly occurs in the large intestine, where is abundant in gut microbiota (Shalon, *et al*., 2023; Kaska, *et al*., 2016). Alterations in intestinal flora act as a critical function in the conversion of primary BAs to secondary BAs, indirectly activating or deactivating membrane and nuclear receptors through the structure modification of the BA, then influence glucose metabolism in humans (Kaska, *et al*., 2016; Fiorucci and Distrutti, 2015). Therefore, we hypothesize that the intestinal flora of model mice is in a state of disorder according to the increased level of CA in the plasma of model mice, and this may be an important mechanism of PE against PCa through modulation of the intestinal flora. Recent research has shown that intestinal flora can regulate physiological processes such as metabolism,

inflammatory responses and immunity. Specifically, the relationship of intestinal flora and malignant tumors has attracted scientific interest and recent investigations have reported the relationship between prostate cancer and the gut and urogenital flora (Wheeler and Liss, 2019). To date, it is unclear whether and how PE can regulate the intestinal flora of prostate cancer and we will explore this problem in future work.

CONCLUSION

Our investigation identified 71 endogenous metabolites as the potential biomarkers in the DU-145 mouse xenograft tumor model, and found that 36 of which were regulated in the treatment group after administrated with PE. These regulated metabolites were mainly linked to the metabolism of amino acids, fatty acids, and bile acids. Overall, the current study provided a further understanding of the anti-PCa mechanism of PE and provided the basis for the development of new antitumor drugs.

ACKNOWLEDGEMENTS

This work was financially supported by National Natural Science Foundation of China (No. 82174108) and Natural Science Foundation of Anhui Province (No. 1808085MH248).

REFERENCES

Bray F, Ferlay J, Soerjomataram I, Siegel RL, Torre LA and Jemal A (2018). Global cancer statistics 2018: GLOBOCAN estimates of incidence and mortality worldwide for 36 cancers in 185 countries. *CA Cancer J. Clin*. **68**: 394-424.

Chen L, Xu YX, Wang YS and Zhou JL (2023). Lipid metabolism, amino acid metabolism and prostate cancer: A crucial metabolic journey. *Asian J. Androl.,* **26**(2): 123-134.

Chen W, Zheng R, Baade PD, Zhang S, Zeng H, Bray F, Jemal A, Yu XQ, He J (2016). Cancer statistics in China, 2015. *CA Cancer J. Clin.,* **66**: 115-132.

Claudio F (2016). Targeting the PI3K/AKT/mTOR pathway in prostate cancer development and progression: insight to therapy. *Clin. Cancer Drugs*, **3**: 36-62.

Cortesi F, Delfanti G, Grilli A, Calcinotto A, Gorini F, Pucci F, Lucianò R, Grioni M, Recchia A, Benigni F, Briganti A, Salonia,A, De Palma M, Bicciato S, Doglioni C, Bellone M, Casorati G and Dellabona P (2018). Bimodal CD40/Fas-dependent crosstalk between iNKT cells and tumor-associated macrophages impairs prostate cancer progression. *Cell Reports,* **22**(11): 3006-3020.

Fei H, Hou J, Wu Z, Zhang L, Zhao H, Dong X and Chen Y (2016). Plasma metabolomic profile and potential biomarkers for missed abortion. *Biomed. Chromatogr*., **30**(12): 1942-1952.

Fiorucci S and Distrutti E (2015). Bile acid-activated receptors, intestinal microbiota and the treatment of metabolic disorders. *Trends Mol. Med*., **21**: 702-714.

Gallimore AM and Godkin A (2013). Epithelial barriers, micro biota and colorectal cancer. *N. Engl. J. Med.,* **368**: 282-284.

Han B, Qi M, Tan WW and Yang MY (2015). Castration-resistant prostate cancer: Current understanding of mechanisms and emerging novel agents. *J. Shandong Univ.* (Health Sci), **53**: 1-7.

Hoang KG, Allison S, Murray M and Petrovic N (2015). Prostanoids regulate angiogenesis acting primarily on IP and EP4 receptors. *Microvasc. Res.,* **101**: 127-134.

Kaska L, Sledzinski T, Chomiczewska A, Dettlaff-Pokora A and Swierczynski J (2016). Improved glucose metabolism following bariatric surgery is associated with increased circulating bile acid concentrations and remodeling of the gut micro biome. *World J. Gastroenterol*., **22**(39): 8698-8719.

Li Y, Pan J and Gou M (2019). The anti-proliferation, cycle arrest and apoptotic inducing activity of peperomin E on prostate cancer PC-3 cell line. *Molecules*, **24**: 1472.

Li Y, Zhang J and Liu M (2018). Chemical constituents of *Peperomia cavaleriei*. *Chem. Nat. Compd.,* **54**: 175-177.

Lin M, Zhu Q, Li Y and Pan J (2021). Peperomin E induces apoptosis and cytoprotective autophagy in human prostate cancer DU145 cells *in vitro* and *in vivo*. *Planta Med*. **87**(8): 620-630.

Lin MG, Yu DH, Wang QW, Lu Q, Zhu WJ, Bai F, Li GX, Wang XW, Yang YF, Qin XM, Fang C, Chen HZ and Yang GH (2011). Secolignans with antiangiogenic activities from *Peperomia dindygulensis*. *Chem Biodivers.,* **8**: 862-871.

Lucarelli G, Rutigliano M, Galleggiante V, Giglio A, Palazzo S, Ferro M, Simone C, Bettocchi C, Battaglia M and Ditonno P (2015). Metabolomic profiling for the identification of novel diagnostic markers in prostate cancer. *Expert Rev. Mol. Diagn.,* **15**: 1211-1224.

Luzzago S, Palumbo C, Rosiello G, Pecoraro A, Deuker M, Stolzenbach F, Mistretta FA, Tian Z, Musi G, Montanari E, Shariat S F, Saad F, Briganti A, de Cobelli O and Karakiewicz PI (2021). Metabolic syndrome predicts worse perioperative outcomes in patients treated with radical prostatectomy for non-metastatic prostate cancer. *Surg. Oncol.,* **37**: 101519.

Nie C, He T, Zhang W, Zhang G and Ma X (2018). Branched chain amino acids: Beyond nutrition metabolism. *Int. J. Mol. Sci*., **19**: 954.

Poulose N, Amoroso F, Steele RE, Singh R, Ong CW and Mills IG (2018). Genetics of lipid metabolism in prostate cancer. *Nat. Genet.,* **50**: 169-171.

Sachan R, Kundu A, Jeon Y, Choi WS, Yoon K, Kim IS, Kwak JH and Kim HS (2018). Afrocyclamin A, a triterpene saponin, induces apoptosis and autophagic cell death via the PI3K/Akt/mTOR pathway in human prostate cancer cells. *Phytomedicine,* **51**: 1139-1150.

Salvado MD, Alfranca A, Haeggström JZ and Redondo JM (2012). Prostanoids in tumor angiogenesis: Therapeutic intervention beyond COX-2. *Trends Mol. Med.,* **18**: 233-243.

Senga S, Kobayashi N, Kawaguchi K, Ando A and Fujii H (2018). Fatty acid-binding protein 5 (FABP5) promotes lipolysis of lipid droplets, de novo fatty acid (FA) synthesis and activation of nuclear factor-kappa B (NF-κB) signaling in cancer cells. *Biochim. Biophys. Acta Mol. Cell Biol. Lipids,* **1863**: 1057-1067.

Shalon D, Culver RN, Grembi JA, Folz J, Treit PV, Shi H, Rosenberger FA, Dethlefsen L, Meng X, Yaffe E, Aranda-Díaz A, Geyer PE, Mueller-Reif JB, Spencer S, Patterson A D, Triadafilopoulos G, Holmes SP, Mann M, Fiehn O, Relman DA and Huang KC (2023). Profiling the human intestinal environment under physiological conditions. *Nature,* **617**(7961): 581-591.

Taha AY, Blanchard HC, Cheon Y, Ramadan E, Chen M, Chang L and Rapoport SI (2017). Dietary linoleic acid lowering reduces lipopolysaccharide-induced increase in brain arachidonic acid metabolism. *Mol. Neurobiol*., **54**: 4303-4315.

Wang XZ, Cheng Y, Wu H, Li N, Liu R, Yang XL, Qiu YY, Wen HM and Liang JY (2016). The natural secolignan peperomin E induces apoptosis of human gastric carcinoma cells via the mitochondrial and PI3K/Akt signaling pathways *in vitro* and *in vivo. Phytomedicine,* **23**: 818-827.

Watt MJ, Clark AK, Selth LA, Haynes VR, Lister N, Rebello R, Porter LH, Niranjan B, Whitby ST, Lo J, Huang C, Schittenhelm RB, Anderson KE, Furic L, Wijayaratne PR, Matzaris M, Montgomery MK, Papargiris M, Norden S, Febbraio M, Risbridger GP, Frydenberg M, Nomura DK and Taylor RA (2019). Suppressing fatty acid uptake has therapeutic effects in preclinical models of prostate cancer. *Sci. Transl. Med.,* **478**: eaau5758.

Wheeler KM and Liss MA (2019). The microbiome and prostate cancer risk. *Curr. Urol. Rep*., **20**: 66.

Yang P, Cartwright CA, Li J, Wen S, Prokhorova IN, Shureiqi I, Troncoso P, Navone NM, Newman RA and Kim J (2012). Arachidonic acid metabolism in human prostate cancer. *Int. J. Oncol.,* **41**: 1495-1503.

Zhang P, Yang X, Wang L, Zhang D, Luo Q and Wang B (2019). Over expressing miR 335 inhibits DU145 cell proliferation by targeting early growth response 3 in prostate cancer. *Int. J. Oncol.,* **54**: 1981-1994.

Table S1: Potential biomarkers from the DU145 cell xenografts in nude mice model and modulation by PE

No.	Var ID	m/z	rt(min)	Mode	Metabolite	Formula	Ion	Mass	CAS	VIP[1-2]	p(anova)	P(1-2)	FC(2/1)	P(2-3)	FC(3/2)
1	M140T46	140.0649	0.76	POS	Betaine	C5H11NO2	[M+Na]+	117.08	590-46-5	2.74	5.51E-18	2.63E-02	1.12	5.10E-09	0.31
2	M154T46	154.0554	0.76	POS	Creatine	C4H9N3O2	[M+Na]+	131.07	57-00-1	1.56	9.83E-04	1.18E-02	0.87	6.48E-01	0.95
3	M156T46	156.0392	0.77	POS	Indoxyl	C8H7NO	[M+Na]+	133.05	480-93-3	1.49	3.40E-07	1.54E-02	1.18	1.95E-07	0.64
4	M136T47	136.0450	0.78	POS	L-Homocysteine	C4H9NO2S	[M+H]+	135.04	6027-13-0	1.08	9.33E-15	6.57E-03	0.90	5.13E-09	0.64
5	M313T47	313.0487	0.78	NEG	Homocystine	C8H16N2O4S2	[M+FA-H]-	268.06	462-10-2	1.13	1.60E-08	1.49E-04	1.48	1.38E-08	0.44
6	M130T66	130.0861	1.10	NEG	L-Leucine	C6H13NO2	[M-H]-	131.09	61-90-5	1.36	1.46E-02	4.03E-02	1.25	2.20E-02	0.78
7	M250T67	250.0754	1.12	POS	Deoxycytidine	C9H13N3O4	[M+Na]+	227.09	951-77-9	1.68	1.38E-18	9.82E-03	0.84	5.10E-09	0.13
8	M115T94	115.0389	1.57	NEG	α-ketoisovaleric acid	C5H8O3	[M-H]-	116.05	759-05-7	1.37	1.65E-02	2.92E-02	0.63	3.63E-02	1.56
9	M265T94	265.1073	1.57	POS	Thiamine	C12H16N4OS	[M+H]+	264.10	59-43-8	1.91	4.49E-08	1.17E-02	0.81	1.89E-04	0.66
10	M307T112	307.0604	1.87	POS	Xanthosine	C10H12N4O6	[M+Na]+	284.08	146-80-5	1.43	2.01E-05	1.42E-03	0.43	3.05E-01	0.49
11	M103T115	103.0512	1.92	POS	L-Phenylalanine	C9H11NO2	Fragment	165.0790	63-91-2	1.11	1.06E-04	8.93E-03	0.79	7.80E-05	1.41
12	M209T121	209.0881	2.02	POS	L-Kynurenine	C10H12N2O3	[M+H]+	208.08	343-65-7	1.63	5.20E-11	1.04E-02	0.77	5.15E-09	1.99
13	M129T198	129.0544	3.29	NEG	Ketoleucine	C6H10O3	[M-H]-	130.06	816-66-0	1.69	1.25E-03	4.25E-03	0.70	9.92E-01	0.99
14	M246T249	246.1654	4.15	POS	2-Methylbutyroylcarnitine	C12H23NO4	[M+H]+	245.16	31023-25-3	4.44	1.06E-07	1.73E-02	0.82	2.95E-04	0.68
15	M180T255	180.0620	4.26	POS	N-ACETYLPROLINE	C7H11NO3	[M+Na]+	157.07	1074-79-9	2.71	4.94E-15	4.65E-04	0.79	5.17E-09	0.38
16	M105T255	105.0307	4.26	POS	Hippuric acid	C9H9NO3	Fragment	179.06	495-69-2	1.56	9.23E-16	9.99E-04	0.81	5.11E-09	0.37
17	M202T279	202.0826	4.65	POS	L-Homophenylalanine	C10H13NO2	[M+Na]+	179.0946	943-73-7	1.12	1.84E-18	1.18E-04	0.76	5.10E-09	0.11
18	M190T394	190.0828	6.57	POS	α-Guanidinoglutaric Acid	C6H11N3O4	[M+H]+	189.0750	73477-53-9	1.63	8.25E-20	4.62E-03	0.86	5.10E-09	0.20
19	M335T398	335.2169	6.64	POS	9-HpODE	C18H32O4	[M+Na]+	312.23	5502-91-0	1.94	3.50E-03	2.93E-03	0.57	4.96E-01	1.24
20	M353T399	353.2270	6.64	POS	Lipoxin B4	C20H32O5	[M+H]+	352.23	98049-69-5	1.04	5.62E-03	4.09E-03	0.58	3.44E-01	1.30
21	M314T400	314.2276	6.66	POS	9-Decenoylcarnitine	C17H31NO4	[M+H]+	313.23		1.51	2.35E-10	8.17E-03	0.68	5.27E-09	2.40
22	M201T414	201.0213	6.91	NEG	7-Methylxanthine	C6H6N4O2	[M+Cl]-	166.05	552-62-5	1.48	2.34E-08	1.42E-02	1.45	1.94E-08	0.18
23	M269T422	269.1353	7.04	POS	Deoxyadenosine	C10H13N5O3	[M+NH4]+	251.10	958-09-8	1.07	8.63E-19	1.75E-04	1.28	5.10E-09	0.12
24	M335T423	335.2169	7.05	POS	11-HpODE	C18H32O4	[M+Na]+	312.23		1.23	5.59E-04	1.63E-03	0.59	9.97E-01	1.01
25	M188T433	188.0697	7.22	NEG	Indole-3-propionic acid	C11H11NO2	[M-H]-	189.08	830-96-6	1.10	3.54E-21	5.19E-05	1.27	5.10E-09	0.06
26	M357T467	357.2730	7.78	POS	Docosatrienoic Acid	C22H38O2	[M+Na]+	334.29	28845-86-5	2.01	2.91E-21	2.74E-05	1.29	5.10E-09	0.05
27	M401T476	401.0845	7.94	NEG	Thr-Asp-OH	C14H16N2O9	[M+FA-H]-	356.09		1.83	7.60E-04	1.54E-03	1.65	3.81E-03	0.64
28	M391T478	391.2090	7.97	NEG	corticosterone	C21H30O4	[M+FA-H]-	346.21		1.41	2.81E-03	8.78E-03	0.40	6.01E-03	2.58
29	M331T487	331.1887	8.11	NEG	PGA3	C20H28O4	[M-H]-	332.20	36614-31-0	1.04	3.42E-11	9.78E-04	0.66	9.80E-07	0.19
30	M676T499	675.5291	8.31	POS	PA(P-16:0/19:0)	C38H75O7P	[M+H]+	674.53		3.89	2.62E-11	1.63E-06	1.74	5.12E-09	0.28
31	M405T500	405.2601	8.34	NEG	7-Ketodeoxycholic acid	C24H38O5	[M-H]-	406.27	911-40-0	1.42	6.45E-15	7.21E-07	1.75	5.10E-09	0.05
32	M297T507	297.2376	8.45	POS	13-HODE	C18H32O3	[M+H]+	296.24	29623-28-7	1.56	6.33E-04	4.50E-04	0.53	2.55E-01	1.34
33	M516T511	516.3001	8.52	POS	Tauroursocholic acid	C26H45NO7S	[M+H]+	515.29	86386-60-9	1.99	6.35E-07	7.16E-03	0.86	4.02E-03	0.82
34	M407T535	407.2762	8.92	NEG	Cholic acid	C24H40O5	[M-H]-	408.29	81-25-4	3.84	2.35E-11	5.17E-04	1.51	5.12E-09	0.15
35	M1066T541	1065.6791	9.01	POS	Ganglioside GA2 (d18:1/16:0)	C54H100N2O18	[M+H]+	1064.70		1.94	1.29E-06	2.35E-02	1.24	7.34E-07	0.55
36	M285T586	285.2168	9.77	POS	Retinaldehyde	C20H28O	[M+H]+	284.21	116-31-4	2.37	1.42E-03	1.14E-03	0.63	4.05E-01	1.20
37	M378T588	378.2377	9.81	NEG	Sphingosine-1-phosphate	C18H38NO5P	[M-H]-	379.25	26993-30-6	1.06	2.00E-04	1.39E-04	0.57	1.96E-01	1.29
38	M305T598	305.2427	9.97	POS	Elaidic acid	C18H34O2	[M+Na]+	282.26	112-79-8	1.36	2.96E-05	4.54E-04	0.47	7.49E-01	0.81
39	M562T600	562.3096	10.00	NEG	LysoPC(18:3)	C26H48NO7P	[M+FA-H]-	517.32		1.09	5.10E-04	2.67E-03	0.68	1.10E-03	1.51
40	M538T611	538.3100	10.18	NEG	LysoPC(16:1)	C24H48NO7P	[M+FA-H]-	493.32		2.14	5.02E-14	1.25E-06	0.73	1.37E-07	0.58
41	M331T618	331.2581	10.31	POS	Eicosadienoic Acid	C20H36O2	[M+Na]+	308.27	122055-58-7	1.80	1.01E-06	2.13E-04	0.43	1.66E-01	0.46
42	M526T622	526.3098	10.37	NEG	LysoPE(18:0/0:0)	C23H48NO7P	[M+FA-H]-	481.32		1.55	1.80E-18	3.10E-04	0.81	5.10E-09	0.25
43	M466T631	466.3232	10.51	POS	LysoPE(P-18:0/0:0)	C23H48NO6P	[M+H]+	465.3219		1.93	3.01E-08	1.09E-03	0.71	1.36E-03	0.61
44	M504T633	504.3048	10.55	NEG	LysoPE(20:2/0:0)	C25H48NO7P	[M-H]-	505.32		1.04	1.60E-03	1.19E-03	0.74	3.33E-01	1.13
45	M588T636	588.3255	10.60	NEG	LysoPC(20:4)	C28H50NO7P	[M+FA-H]-	543.33		2.52	3.06E-07	2.67E-02	0.84	5.25E-04	0.71
46	M1036T656	1035.6527	10.94	NEG	LysoPC(16:0)	C24H50NO7P	[2M+FA-H]-	495.33		1.89	2.44E-02	4.54E-02	0.73	1.00E+00	1.00
47	M436T674	436.2792	11.24	NEG	PE(P-16:0/0:0)	C21H44NO6P	[M-H]-	437.29		1.37	5.74E-12	2.26E-04	0.70	4.64E-07	0.37
48	M566T674	566.3411	11.24	NEG	LysoPC(18:1)	C26H52NO7P	[M+FA-H]-	521.35		4.92	5.25E-09	2.38E-04	0.75	1.02E-03	0.70
49	M583T674	583.3311	11.24	NEG	PI(P-18:0/0:0)	C27H53O11P	[M-H]-	584.33		2.04	6.40E-08	2.13E-06	0.64	7.01E-01	0.93
50	M554T691	554.3414	11.52	NEG	LysoPE(20:0/0:0)	C25H52NO7P	[M+FA-H]-	509.35		1.61	1.01E-10	8.11E-03	0.80	4.93E-07	0.50
51	M552T694	552.3957	11.56	POS	LysoPC(20:0/0:0)	C28H58NO7P	[M+H]+	551.40	108341-80-6	1.91	8.30E-08	3.71E-02	0.79	1.06E-04	0.51
52	M319T694	319.2247	11.57	NEG	15-HETE	C20H32O3	[M-H]-	320.24	73836-87-0	6.09	2.26E-03	1.15E-02	0.61	8.90E-01	0.90
53	M387T694	387.2113	11.57	NEG	17-phenyl trinor PGF2α	C23H32O5	[M-H]-	388.23	38344-08-0	1.31	8.92E-06	5.85E-06	0.43	9.01E-02	1.50
54	M841T694	840.5675	11.57	NEG	PE(20:4/20:0)	C45H82NO8P	[M+FA-H]-	795.58		1.20	3.01E-11	9.52E-09	0.40	3.21E-01	0.73
55	M867T694	866.5836	11.57	NEG	PE(22:1)/20:4)	C47H84NO8P	[M+FA-H]-	821.59		1.04	4.08E-11	1.25E-05	0.52	7.83E-05	0.19
56	M592T695	592.3564	11.58	NEG	LysoPC(20:2)	C28H54NO7P	[M+FA-H]-	547.36		1.35	7.35E-15	7.00E-03	0.80	5.12E-09	0.19
57	M843T715	842.5843	11.92	NEG	PE(22:2/18:1)	C45H84NO8P	[M+FA-H]-	797.59		1.38	2.12E-11	5.62E-09	0.25	9.56E-01	0.91
58	M568T728	568.3564	12.13	NEG	LysoPC(18:0)	C26H54NO7P	[M+FA-H]-	523.36		7.39	3.26E-03	9.06E-03	0.71	9.97E-01	0.99
59	M585T728	585.3468	12.13	NEG	PI(O-18:0/0:0)	C27H55O11P	[M-H]-	586.35		2.03	6.79E-03	3.14E-02	0.77	8.59E-01	0.94
60	M594T742	594.3718	12.37	NEG	LysoPC(20:1)	C28H56NO7P	[M+FA-H]-	549.38		1.23	2.78E-14	2.16E-03	0.79	5.27E-09	0.32
61	M582T766	582.3721	12.76	NEG	LysoPE(22:0/0:0)	C27H56NO7P	[M+FA-H]-	537.38		1.01	2.61E-06	3.09E-02	0.78	3.28E-03	0.62
62	M301T775	301.2144	12.92	NEG	Eicosapentaenoic Acid	C20H30O2	[M-H]-	302.22	10417-94-4	2.79	2.20E-04	7.57E-03	1.45	1.96E-04	0.56
63	M277T781	277.2148	13.01	NEG	α-Linolenic Acid	C18H30O2	[M-H]-	278.22	463-40-1	2.26	1.89E-04	1.72E-02	1.34	1.30E-04	0.59
64	M327T800	327.2299	13.33	NEG	Docosahexaenoic acid	C22H32O2	[M-H]-	328.24	6217-54-5	5.61	2.68E-02	2.02E-02	1.54	3.74E-01	0.83
65	M303T810	303.2302	13.50	NEG	Arachidonic Acid	C20H32O2	[M-H]-	304.24	506-32-1	7.54	1.44E-14	3.40E-07	1.67	5.10E-09	0.17
66	M279T818	279.2304	13.63	NEG	Linoleic acid	C18H32O2	[M-H]-	280.24	60-33-3	2.82	1.03E-04	4.09E-02	1.26	6.10E-05	0.60
67	M329T825	329.2454	13.74	NEG	Docosapentaenoic acid	C22H34O2	[M-H]-	330.26	25448-00-4	3.03	5.54E-09	3.09E-05	1.81	8.46E-09	0.28
68	M305T835	305.2456	13.91	NEG	Eicosatrienoic Acid	C20H34O2	[M-H]-	306.26		1.13	9.14E-10	9.34E-04	1.54	5.57E-09	0.20
69	M429T838	429.3669	13.97	POS	1-Hydroxyvitamin D5	C29H48O2	[M+H]+	428.3654		1.35	2.27E-03	2.81E-02	0.58	5.80E-01	0.73
70	M255T849	255.2305	14.16	NEG	Palmitic acid	C16H32O2	[M-H]-	256.24	57-10-3	1.34	6.12E-03	3.87E-02	1.33	6.64E-03	0.68
71	M331T849	331.2610	14.16	NEG	Docosatetraenoic Acid	C22H36O2	[M-H]-	332.27	122068-08-0	1.31	1.87E-06	4.65E-03	1.67	1.03E-06	0.26

rt: Retention time; VIP[1-2] : the contribution value of the metabolite differences between the control (Normal) and model groups.; FC(3/2): The fold change of the drug treatment group compared to the model group; P(2-3): Its value serves as a statistical reference for the significance of metabolites between the treatment and model groups; 1,2,3 respectively refer to the control group, model group, and treatment group.

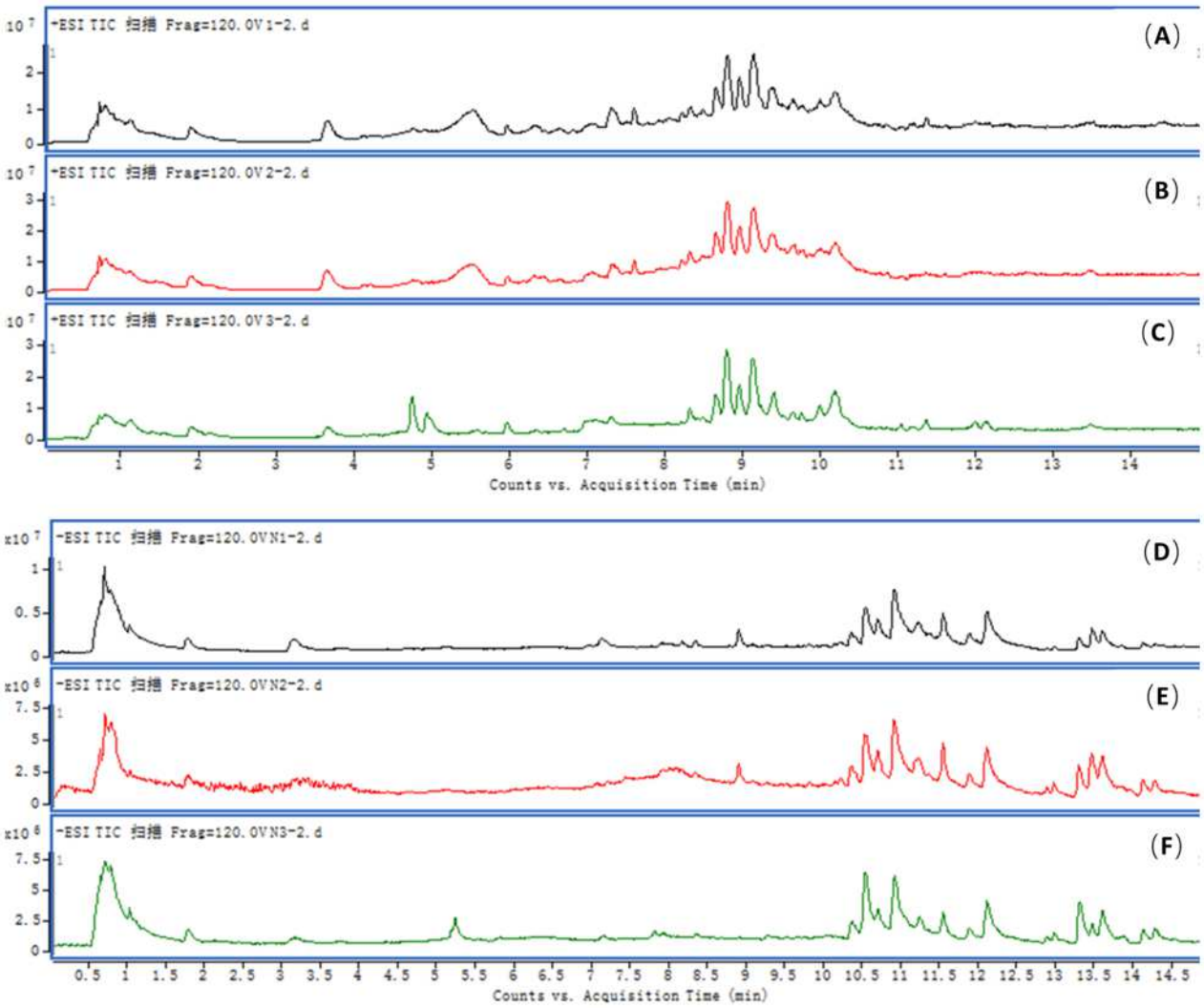

Fig. S1: Representative TICs in positive-ion mode: (A) normal control group, (B) model group, (C) treatment group and in ESI negative-ion mode: (D) control group, (E) model group, (F) treatment group.

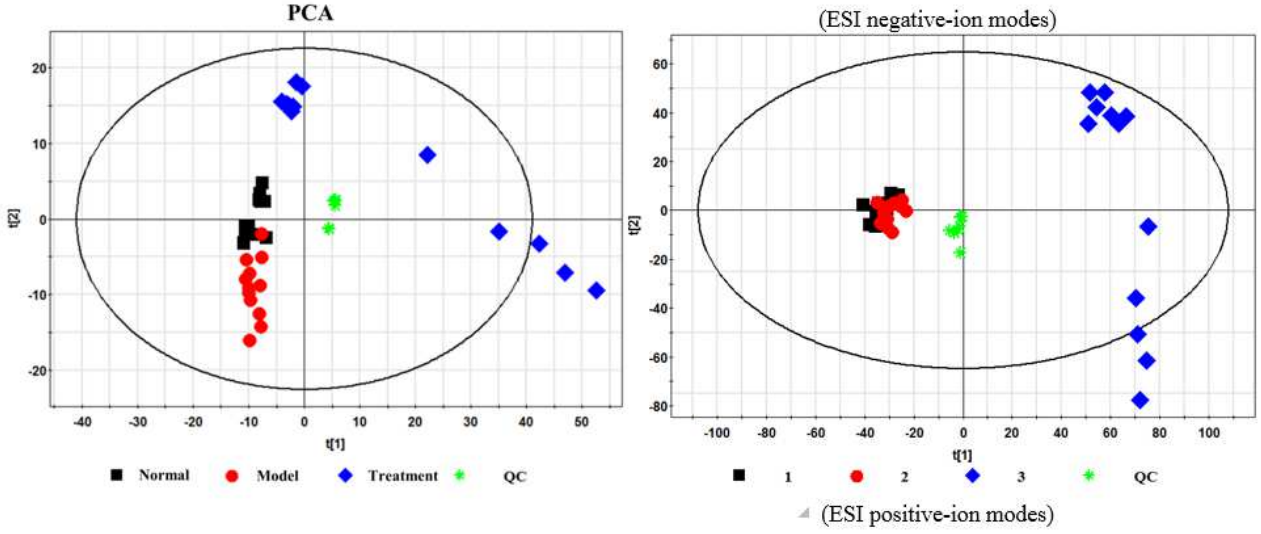

Fig. S2: PCA score plots of four groups (normal group, model group, treatment group and QC) in ESI negative-ion and positive-ion modes.

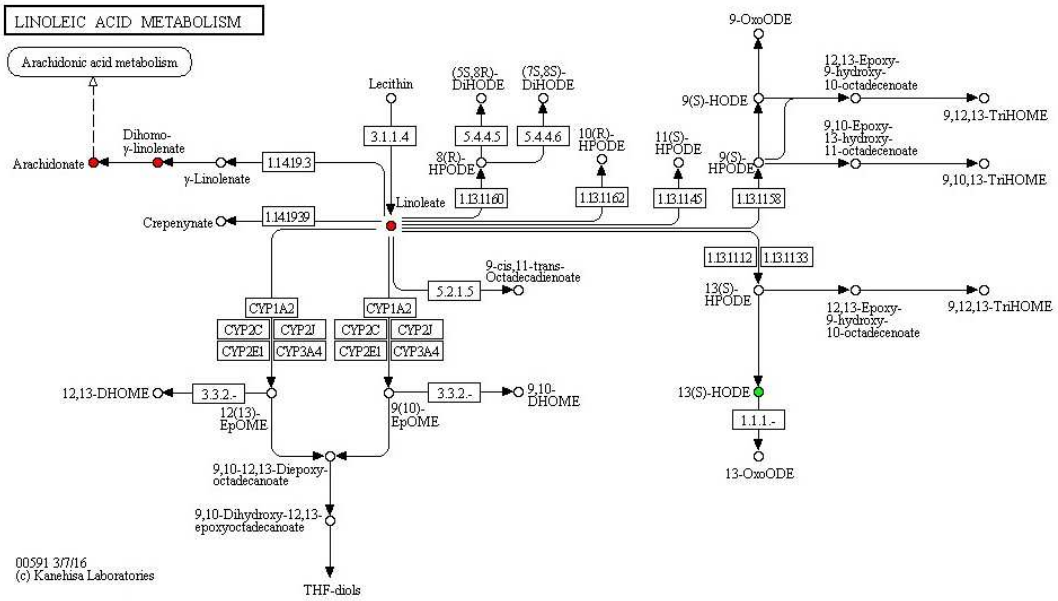

Fig. S3: Linoleic acid metabolism pathway

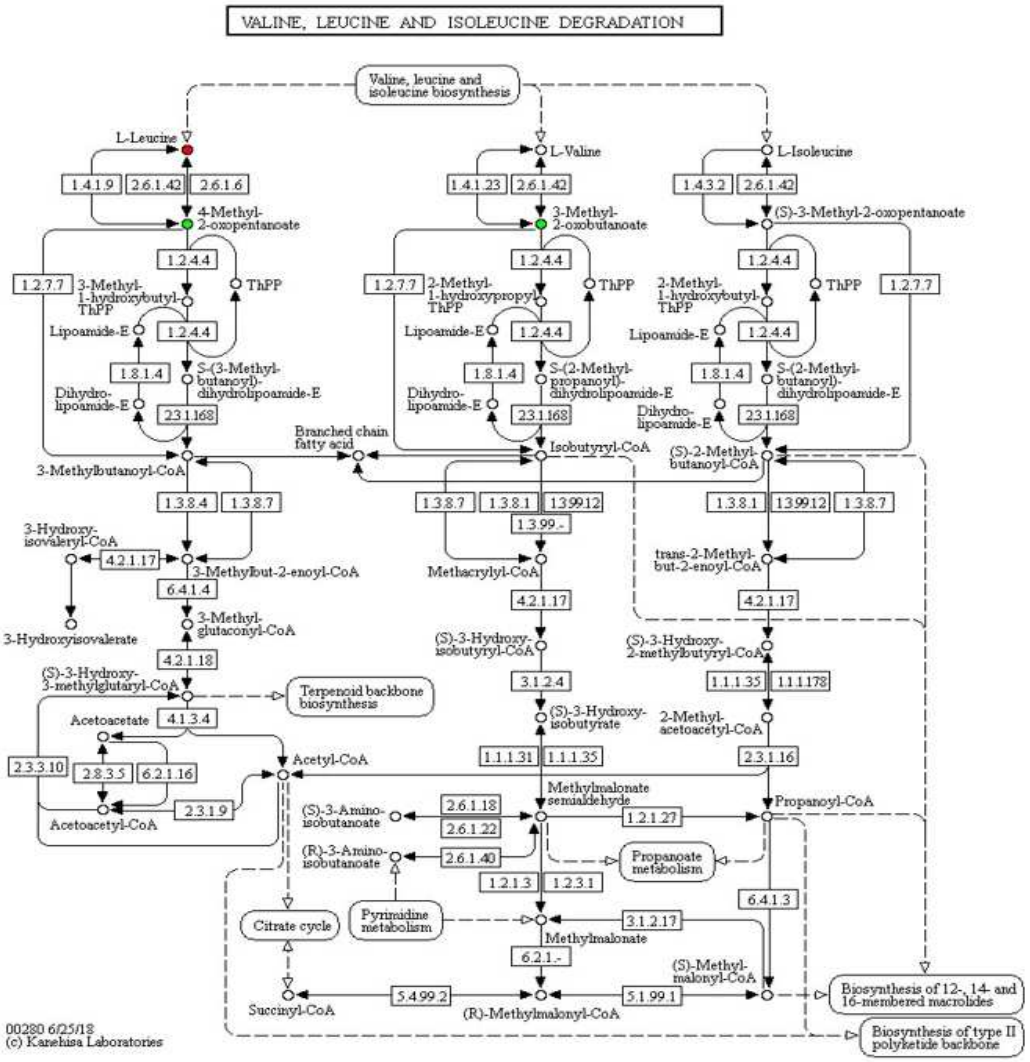

Fig. S4: Valine, leucine and isoleucine degradation

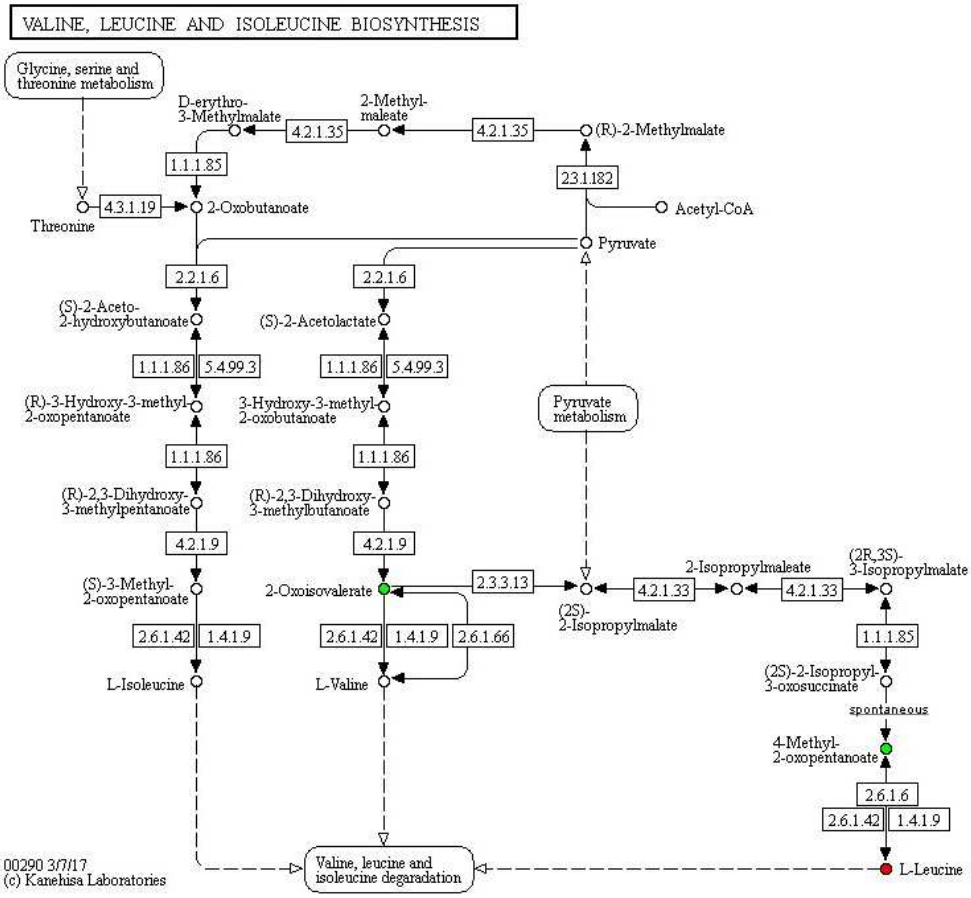

Fig. S5: Valine, leucine and isoleucine biosynthesis

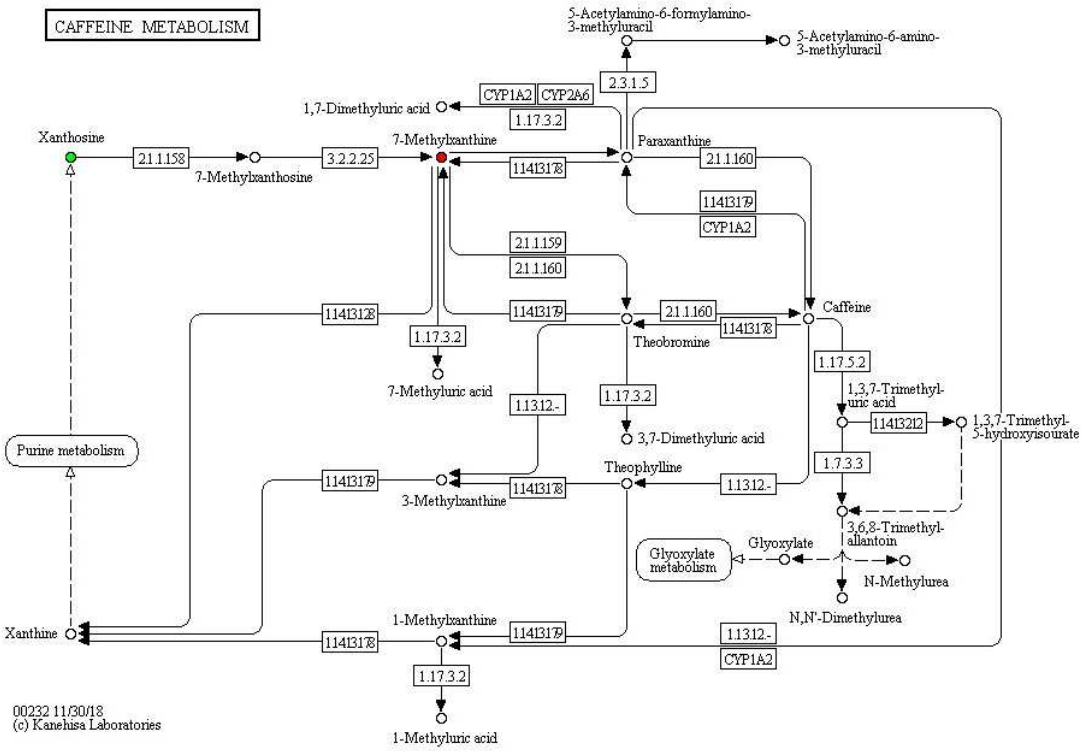

Fig. S6: Caffeine metabolism

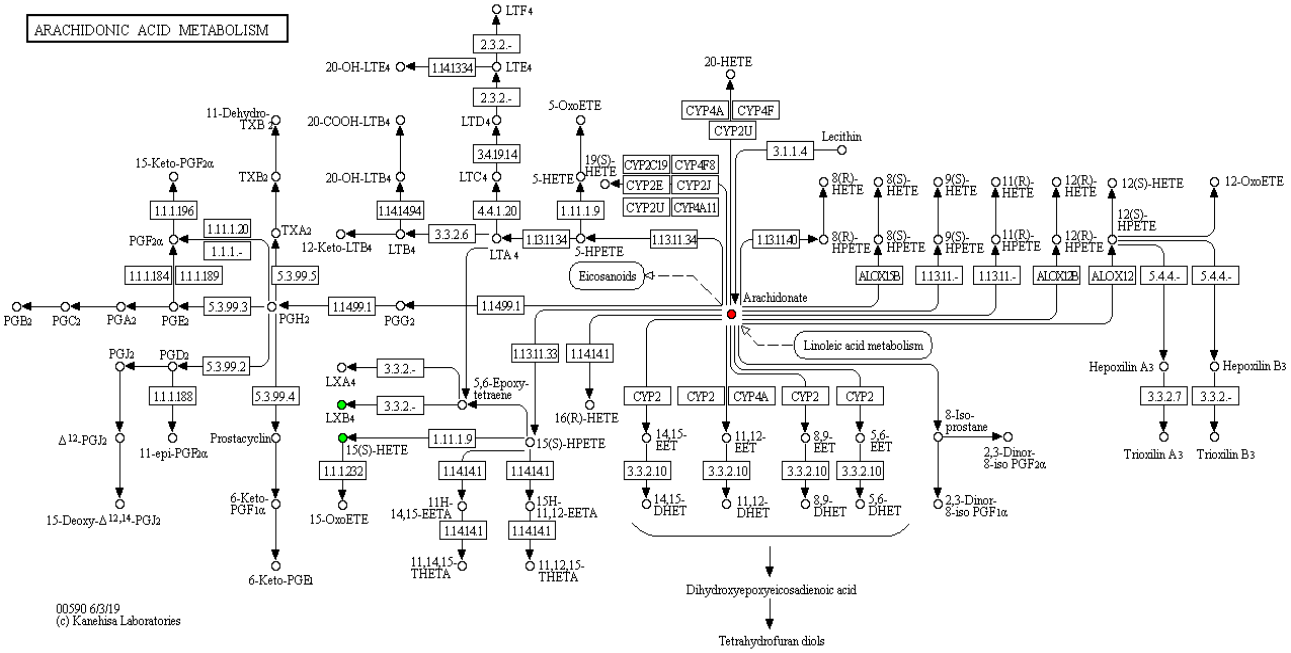

Fig. S7: Arachidonic acid metabolism

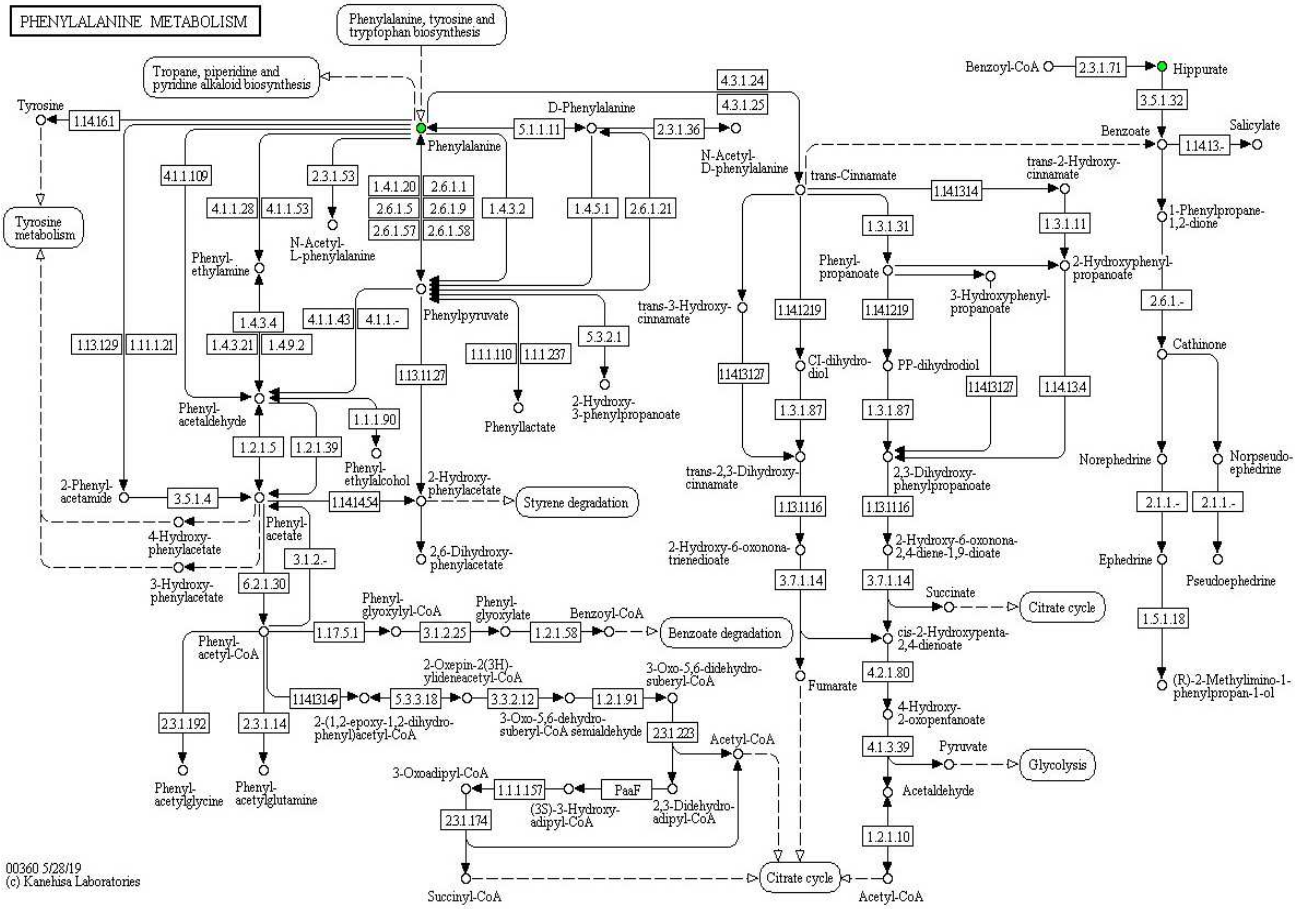

Fig. S8: Phenylalanine metabolism

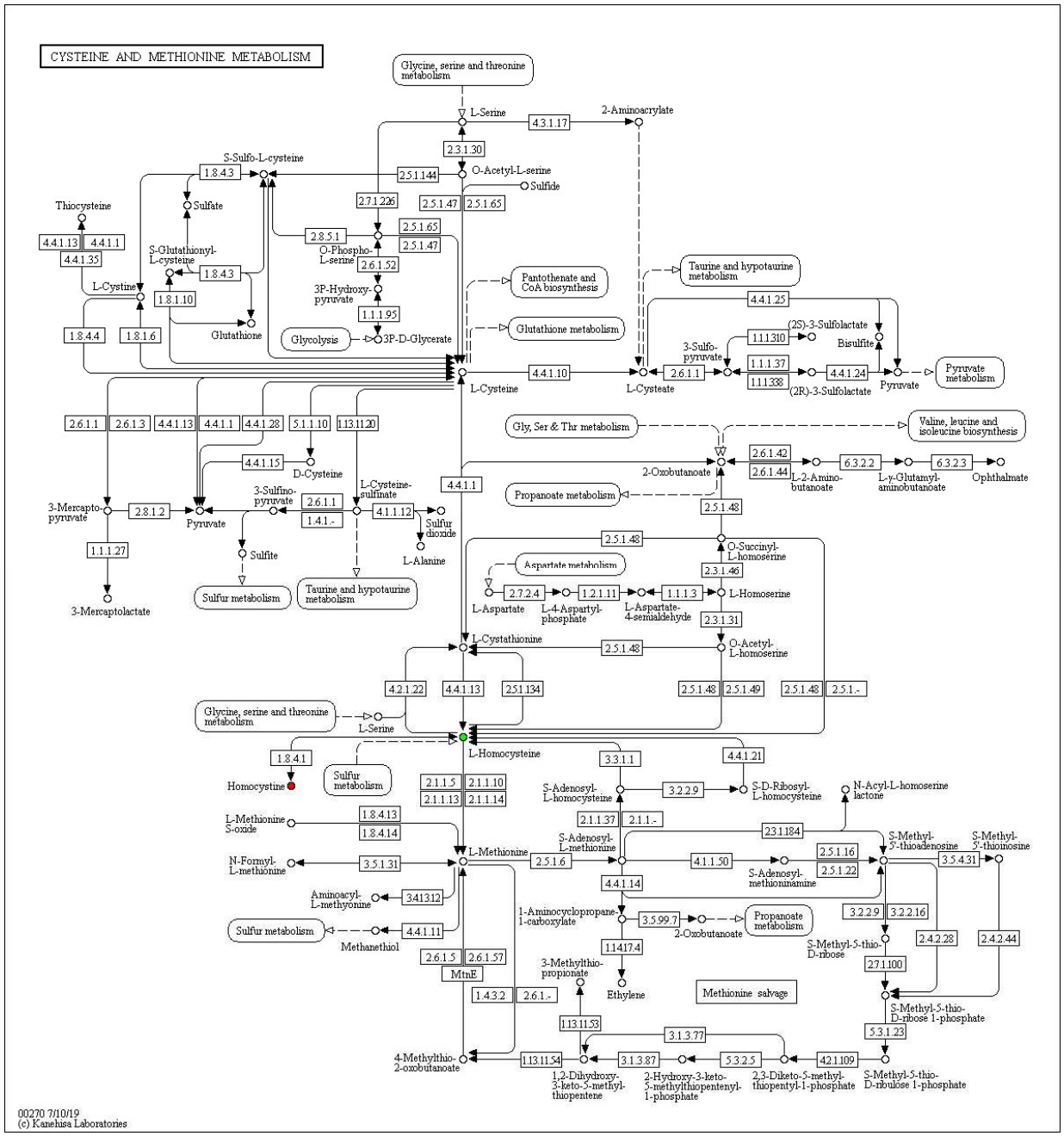

Fig. S9: Cysteine and methionine metabolism